AFWL-TR-82-91

AFWL-TR-
82-91

AD A125976

THEORETICAL MODELING OF EMP EFFECTS IN SEMICONDUCTOR JUNCTION DEVICES

J. H. Yee
W. J. Orvis
L. C. Martin

Lawrence Livermore National Laboratory
Livermore, CA 94550

February 1983

Final Report

Approved for public release; distribution unlimited.

AIR FORCE WEAPONS LABORATORY
Air Force Systems Command
Kirtland Air Force Base, NM 87117

This final report was prepared by the Lawrence Livermore National Laboratory, Livermore, California, under Contract W-7705-ENG-48 and Project Orders 81-037 and 82-101, Job Order 37630146 with the Air Force Weapons Laboratory, Kirtland Air Force Base, New Mexico. Lieutenant Mark E. Snyder (NTAT) was the Laboratory Project Officer-in-Charge.

This report has been reviewed by the Public Affairs Office and is releasable to the National Technical Information Service (NTIS). At NTIS, it will be available to the general public, including foreign nations.

If your address has changed, if you wish to be removed from our mailing list, or if your organization no longer employs the addressee, please notify AFWL/NTAT, Kirtland AFB, NM 87117 to help us maintain a current mailing list.

This technical report has been reviewed and is approved for publication.

Mark E. Snyder

MARK E. SNYDER
2d Lt, USAF
Project Officer

FOR THE COMMANDER

James A. Kee

JAMES A. KEE
Major, USAF
Chief, Technology Branch

Roger S. Case Jr.

ROGER S. CASE, JR.
Lt Colonel, USAF
Chief, Aircraft & Missile Division

DO NOT RETURN COPIES OF THIS REPORT UNLESS CONTRACTUAL OBLIGATIONS OR NOTICE ON A SPECIFIC DOCUMENT REQUIRES THAT IT BE RETURNED.

UNCLASSIFIED

SECURITY CLASSIFICATION OF THIS PAGE (When Data Entered)

REPORT DOCUMENTATION PAGE	READ INSTRUCTIONS BEFORE COMPLETING FORM
1. REPORT NUMBER: AFWL-TR-82-91	2. GOVT ACCESSION NO.: AD-A125976
	3. RECIPIENT'S CATALOG NUMBER:
4. TITLE (and Subtitle): THEORETICAL MODELING OF EMP EFFECTS IN SEMICONDUCTOR JUNCTION DEVICES	5. TYPE OF REPORT & PERIOD COVERED: Final Report
	6. PERFORMING ORG. REPORT NUMBER:
7. AUTHOR(s): J. H. Yee, W. J. Orvis, L. C. Martin	8. CONTRACT OR GRANT NUMBER(s): W-7705-ENG-48, PO 81-037 & 82-101
9. PERFORMING ORGANIZATION NAME AND ADDRESS: Lawrence Livermore National Laboratory, Livermore, CA 94550	10. PROGRAM ELEMENT, PROJECT, TASK AREA & WORK UNIT NUMBERS: 64711F/37630146
11. CONTROLLING OFFICE NAME AND ADDRESS: Air Force Weapons Laboratory (NTAT), Kirtland Air Force Base, NM 87117	12. REPORT DATE: February 1983
	13. NUMBER OF PAGES: 40
14. MONITORING AGENCY NAME & ADDRESS (if different from Controlling Office)	15. SECURITY CLASS. (of this report): Unclassified
	15a. DECLASSIFICATION/DOWNGRADING SCHEDULE:
16. DISTRIBUTION STATEMENT (of this Report): Approved for public release; distribution unlimited.	
17. DISTRIBUTION STATEMENT (of the abstract entered in Block 20, if different from Report):	
18. SUPPLEMENTARY NOTES:	
19. KEY WORDS (Continue on reverse side if necessary and identify by block number): EMP, Semiconductor, Modeling, Second Breakdown	

20. ABSTRACT (Continue on reverse side if necessary and identify by block number):
This report discusses ~~(1)~~ various damage mechanisms and their effects on the performance of semiconductor devices, and ~~(2)~~ some of the important theoretical models which are used to describe second breakdown phenomena. The dominant mechanism responsible for the occurrence of second breakdown is probably the thermal excitation of electrons from a device's valence band (thermal mode second breakdown); conclusions from theoretical calculations based on three different approximations seem to support this model. Current mode breakdown,
(Over)

DD FORM 1 JAN 73 1473 EDITION OF 1 NOV 65 IS OBSOLETE

UNCLASSIFIED

SECURITY CLASSIFICATION OF THIS PAGE (When Data Entered)

20. ABSTRACT (Continued)

another form of second breakdown, is discussed in terms of the role it plays in determining the shape of the threshold failure power curve.

PREFACE

The authors wish to thank Dr. Phil Castillo and Second Lieutenant M. Snyder of the Air Force Weapons Laboratory (AFWL), and Dr. H. Cabayan of Lawrence Livermore National Laboratory for providing valuable information and suggestions during the course of this work.

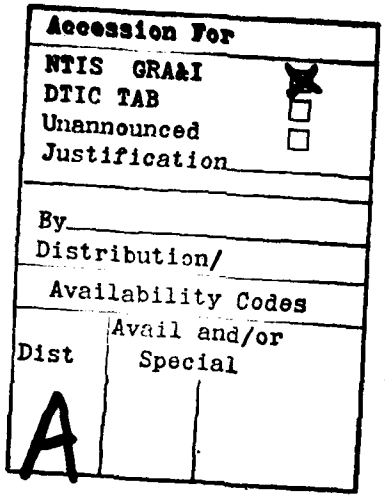

CONTENTS

Section	Page
INTRODUCTION	5
SOME IMPORTANT EXISTING MODELS	6
Wunsch-Bell Model	6
Electrothermal Models	7
PHYSICS OF SECOND BREAKDOWN	11
Thermal Mode Second Breakdown	11
Current Mode Second Breakdown	25
MULTIPLE HOT SPOT FORMATIONS AND THEIR EFFECT ON THE TRANSPORT PARAMETERS OF THE DEVICES	30
SOME RECENT EXPERIMENTAL RESULTS	32
OTHER DAMAGE MECHANISMS	33
Electromigration	33
Electrical Breakdown Between Metalization Strips	35
High Field Surface Breakdown	35
CONCLUSION	37
REFERENCES	38

ILLUSTRATIONS

Figure		Page
1	The Scarlett and Shockley thermal instability mechanism illustrating breakdown during forward bias in some transistors.	9
2	Ionization coefficients for electrons and holes in some typical p-n junction diodes.	15
3	I-V characteristics in the second breakdown region of a p-n junction based on thermal excitation models.	18
4	Energy band diagrams showing the similarity between thermionic emission of electrons of a metal and thermal excitation of electrons out of the valence bands in a semiconductor.	19
5	Steady state current density and temperature as a function of radius in a cylindrical junction at three points in the second breakdown region. ("0" is at the center of the device and "1" is at the edge.)	21
6	Comparison between the experimental and the theoretical resistivity data.	22
7	Configuration of the cylindrical p-n junction used for this analysis.	24
8	Time history of the voltage and current for the diode simulation.	26
9	Current density and temperature during thermal and avalanche breakdown for the diode model. (Each line is for one time step of 1 x 10-4 s.)	27
10	Variation of total current I versus time as a function of terminal voltage V for the current mode and thermal mode second breakdown.	29
11	Explanation of the multiple hot spot formations by the distortions of the energy bands.	31
12	Defect model used in calculating the electric field near the voids.	34
13	Metallization strips voltage breakdown.	36

INTRODUCTION

Electromagnetic Pulses (EMP) coming from such diverse sources as lightning, RADAR beams, or nuclear explosions, can induce transient electrical effects in metallic or semiconductor materials. Damage to sensitive components by strong EMP-induced transients is a serious problem in both military and commercial electronic systems. While many circuits can be protected from EMP by metal boxes, others require connections to wires that must pass out of these boxes. These wires act as antennas and channel the destructive pulses through the shield and into the electronics. Invariably, some of these penetrating wires connect directly to sensitive electronic components (e.g., the signal diode in a communications system that must connect to an antenna wire). If the system is to survive, these components must be able to withstand the EMP induced transient with a minimum of damage or degradation.

Solid-state electronic circuits contain many physical components (i.e., resistors, capacitors, diodes, transistors, metal strips, etc.), all of which can be destroyed or degraded by an EMP. For example, a high voltage pulse can cause two closely spaced metal strips to short, or induce a conduction path through an insulator. Understanding the effects of EMP on the various circuit components is essential to be able to answer questions concerning the operability or survivability of a particular circuit or system in an EMP environment.

There are many different types of damage mechanisms that can occur in electronic components. Semiconductors can experience thermal and current mode second breakdown, surface breakdown, electromigration of impurity atoms, and many other high-field effects. Insulators can experience bulk or surface breakdown. Wires can be attracted towards each other to cause a short, or simply be burned off.

This report discusses these damage mechanisms and their effects on the performance of semiconductor devices. The failure levels of sensitive electronic devices such as semiconductors can vary over a wide range of amplitudes; and any hardening approach of a complex system with a very large number of such devices must take this wide variability of failure levels into consideration. If the hardening strategy places its emphasis on using harder devices with minimum tolerances in variability, the question arises as to how this can be accomplished. For example, for semiconductor devices, you may want to increase mean failure levels and minimize the spread about these levels. This may require establishing certain tolerance limits on the physics parameters that affect the manufacturing of such devices. However, with the present level of knowledge of failure mechanisms, this is not possible. Almost all presently used analysis techniques are semi-empirical in nature, and the relationships between the physics mechanisms and the failure levels is not well known.

The purpose of this investigation is, therefore, to assess the existing models and known mechanisms which can cause damage to a p-n junction device in an EMP environment. After this, we will try to extend the existing models to a form which will be capable of accurately predicting the failure power for p-n junction devices.

SOME IMPORTANT EXISTING MODELS

The physical phenomenon which leads to internal damage in junction devices is second breakdown. The onset of second breakdown appears to be associated with an instability in which the current tends to concentrate in a small filament, rather than spread uniformly over the whole junction area. This phenomenon occurs whenever the input voltage reaches certain threshold values. Experiments show that second breakdown does not always damage the device. It only does so if the device operates in the second breakdown mode for a period of time. For example, if a second breakdown occurs and the input power is quickly reduced below the threshold levels, there is evidence that the device will return to its normal operating condition.

Various theories and models proposed in the last 20 years try to explain such phenomena. These theories are generally grouped into two categories--thermal models and electrothermal models. The following subsections will describe some of these models in detail.

WUNSCH-BELL MODEL

In this model (Ref. 1), joule heating is produced as current flows through a potential difference at the junction. This heating raises the junction temperature until melting occurs. The Wunsch-Bell Model can handle either adiabatic (short time), quasi-adiabatic (intermediate times), or thermal equilibrium (long time) systems. Many difficulties exist with this model. It contains many parameters which are usually not accurately known. In applying this model to predict failure power, you often assume that the critical temperature is that temperature at which the doping concentration is equal to the intrinsic carrier concentration. However, when second breakdown occurs, temperature of the device is so high that the intrinsic carrier concentration can be much higher than that of the doping concentration. When second breakdown occurs, the current tends to flow through one or more channels, which occurs even in homogeneous junctions (Ref. 2). The Wunsch-Bell model does not take this channeling phenomenon into consideration. It is based on the assumption that the current flows uniformly throughout the junction (Ref. 3). Therefore, we do not expect this model to very accurately predict the threshold power.

In order to accurately predict the threshold power for any semiconductor device, you must simultaneously solve the continuity equations for electrons and holes, Poisson's equation, and the thermal energy transport equation. Wunsch and Bell used only the thermal-energy transport equation and ignored all the couplings between electrons, holes, and phonons in the crystal. All of the detailed physics of the problem are lumped into the model's constants. As a result, this model does not have the capability to be used for investigating the sensitivity of the failure power to variations in the physical parameters.

It has been known for some time that two second breakdown phenomena exist in transistor devices (Ref. 4). One is thermal second breakdown, and the other is current mode second breakdown. The latter is an electronic phenomenon

with a delay time to onset on the order of nanoseconds. Therefore, any attempt to use the Wunsch-Bell model to predict breakdown phenomena when a transistor is subjected to a pulse with a pulse width in the nanosecond range may be entirely incorrect. Kalab (Ref. 5) and Kleiner (Ref. 6) have both observed that the plots of critical power as a function of pulse width in the short pulse width region (10 ns or less) were quite different from those predicted by the Wunsch-Bell model.

ELECTROTHERMAL MODELS

A more sophisticated model is called the electrothermal model. It was recently used by Ward (Ref. 7) to investigate second breakdown phenomena in p-n junction devices. In this model, the transport equations of the electrons and holes and the energy equation for the temperature are solved simultaneously using a computer. Even though Ward had only considered the one-dimensional case, he was able to obtain a power failure curve that agrees very well with some of the experimental data of Tasca, et al. (Ref. 8). In principle, the approach used by Ward should be able to more accurately describe second breakdown mechanisms than the Wunsch-Bell Model. However, in order to describe the filament formation and other physical phenomena associated with second breakdown, you must extend the calculation to two or three dimensions. In addition, the calculation must also be extended to higher temperatures than those considered by Ward.

At the present time, accurate avalanche coefficients for electrons and holes are not known for temperatures greater than 400 K. Therefore, work also should be done to theoretically and experimentally determine these coefficients at higher temperatures.

Another electrothermal model was recently employed by Barush and Budenstein (Ref. 9). In this model, the device is divided into small square segments. Instead of solving the transport equations of the electrons and holes for each segment, Barush and Budenstein used a set of equivalent circuit equations to relate the current and the voltage in each segment to the total voltage and current. The thermal portion of the problem is solved by equating the increase in the internal energy in each segment to the algebraic sum of the heat added to each segment from the four surrounding square segments and the substrate, plus joule heating from the current flowing through the segment. In this calculation, the voltage as a function of the temperature is needed from an experiment.

A two-step progression in conjunction with an iterative procedure was employed to establish the current and temperature distributions. The important result obtained from this calculation is that it shows that hot spot formation does exist, even for a homogeneous junction. For the junction with inhomogeneities or damage, the hot spots form at a lower current density. Because the theory does not take into consideration the exact doping density and other things such as the convergence of the current lines, the theoretical results do not agree quantitatively with the experimental ones. Since the transport

properties of the electrons and holes are replaced by a set of circuit equations, this model again does not directly explain the physics of second breakdown, but it does show that hot spot formation occurs even in homogeneous devices.

Another model which combines the electrical and thermal properties of p-n junctions has recently been investigated by Kusnezov and Smith (Ref. 10). In this model, the physics of the junction model was converted to an equivalent electrical and thermal circuit. The procedure for determining the electrical characteristics is, first, to use the electrical model to calculate the instantaneous power dissipation with the structure at a uniform temperature. The power dissipation is then inserted into the thermal model and the temperature allowed to rise for a specified period of time. At this point, a new set of node temperatures is developed. Using these new temperatures, the thermal conductivity and the resistivity is calculated along with the new forward voltage. By iterating between the two models, they obtain the power density as a function of distance in the devices, and the failure power as a function of the delay time. Up to now, the results obtained from this model are only qualitative.

The agreement between the calculated results and experiments is very poor. Again, because of the macroscopic nature of the theor the physics of second breakdown is buried in the parameters used in the ca ation.

In addition to the various models described in the pre s sections, Hower (Ref. 11) used a model based on ideas of Shockley and rlett (Ref. 12). The model uses the concept of the stability factor S, defin the following equation:

$$S = R_{TH} V_{ce} \frac{\partial I_c}{\partial T} \tag{1}$$

where V_{ce}, I_c and R_{TH} are the collector-to-emitter voltage, collector current, and the thermal resistance, respectively. The device is thermally stable when

$$S \leq 1 \tag{2}$$

and thermally unstable when

$$S > 1 \tag{3}$$

Using the conditions given in Equations 2 and 3, and the equations which describe the current and voltage for a junction device, you can obtain a locus of stability as shown in Figure 1. According to Hower (Ref. 13), in the region below the locus of the stability curve, the current is uniform and there is no hot spot formation. Above the stability curve, hot spots occur.

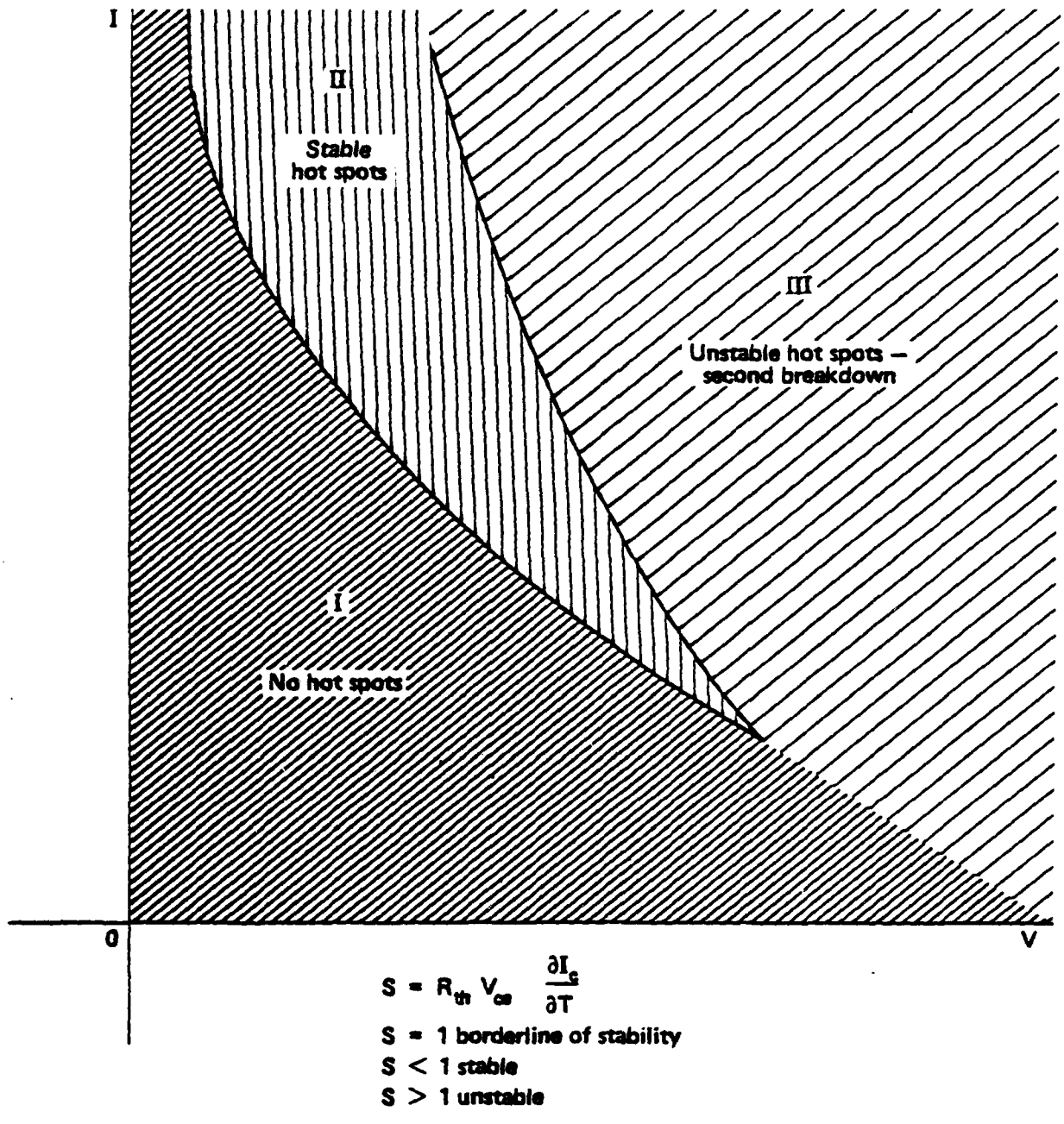

Figure 1. The Scarlett and Shockley thermal instability mechanism illustrating breakdown during forward bias in some transistors.

If the current or voltage continues to increase, the device can be taken into the region where second breakdown occurs. The theoretical results of Hower have been verified experimentally for a number of transistor devices (Refs. 11,13) for the case of steady state input power. At this point, whether Hower's results are applicable to EMP situations is not clear. Certainly using the stability factor concept to define the areas of safe operation for a device is a very appealing idea.

In the future, the applicability of this concept to the EMP problems will be considered.

PHYSICS OF SECOND BREAKDOWN

THERMAL MODE SECOND BREAKDOWN

Although many models have been used in the past to explain the mechanisms of second breakdown, none describes the real physical processes responsible for this phenomenon. Some of the theoretical calculations involve lengthy computer calculations and others are based upon too many assumptions. As a result, the physics of second breakdown are lost through computation procedures. The following section will present, in the simplest way, how the second breakdown phenomena may occur. Since second breakdown or any damage mechanism is a very complicated phenomenon, assumptions and approximations are necessary to reduce the complicated equations to a simple form so that a meaningful physical model will result.

In theory, you can investigate second breakdown phenomena by the following set of differential equations.

The continuity equations for electron (n) and hole (p) densities:

$$e\frac{\partial n}{\partial t} = +\nabla J_n + \alpha J_n + \beta J_p - eR(n,p) \tag{4}$$

$$e\frac{\partial p}{\partial t} = -\nabla J_p + \alpha J_n + \beta J_p - eR(n,p) \tag{5}$$

where the current densities are expressed by,

$$J_p = pe\mu_p E - eD_p \nabla P \tag{6}$$

$$J_n = ne\mu_n E + eD_n \nabla n \tag{7}$$

Poisson's equation:

$$\nabla \cdot \bar{E} = e(n-p+N)/\epsilon_o \tag{8}$$

The heat flow equation:

$$\rho c \frac{dT}{dt} = \bar{J} \cdot \bar{E} + \bar{\nabla} \cdot [K(\bar{x},t)\nabla T] \tag{9}$$

where

α = electron ionization coefficient

β = hole ionization coefficient

μ_n = electron mobility

μ_p = hole mobility

R = recombination rate

e = charge on an electron

J_n = electron current density

J_p = hole current density

n = electron concentration

p = hole concentration

E = electric field

N = net ionized impurities

$K(\bar{x},t)$ = thermal conductivity

ϵ = dielectric constant

ρ = mass density

c = specific heat

Equations 4 through 9 are very complicated to solve analytically. Therefore, in order to gain some insight into the physical processes involved in breakdown phenomena, we consider some simple cases.

As a start, we will consider a one-dimensional steady state solution. In this case, the electron, hole, and current densities are constants, and the gradients reduce to derivatives of a single variable. Therefore:

$$\frac{\partial n}{\partial t} = \frac{\partial p}{\partial t} = 0 \tag{10}$$

$$J = J_n + J_p = \text{constant} \tag{11}$$

$$\nabla \cdot J_n = \frac{dJ_n}{dx} \tag{12}$$

$$\nabla \cdot J_p = \frac{dJ_p}{dx} \tag{13}$$

Inserting Equations 10 to 13 into Equations 4 and 5 gives

$$\frac{dJ_p}{dx} = \beta J_p + \alpha J_n - eR(n,p) \tag{14}$$

$$\frac{dJ_n}{dx} = -\beta J_p - \alpha J_n + eR(n,p) \tag{15}$$

Now, assuming a single trap at the center of the forbidden band, the recombination-generation terms R(n,p) can be determined from (Ref. 14):

$$R(n,p) = \frac{(pn - n_i^2)}{(n + n_i)\tau_p + (p + n_i)\tau_n} \tag{16}$$

n_i = intrinsic carrier density

τ_n, τ_p = electron and hole effective lifetimes

For the case of a reverse biased p-n junction, where $n_i > n,p$, this equation can be approximated with

$$R(n,p) \quad \frac{-n_i}{\tau_n} \tag{17}$$

Solving Equation 11 for J_n, inserting it into Equation 14, and multiplying by the area (A) to get the current, gives

$$\frac{dI_p}{dx} + I_p(\alpha-\beta) = \alpha I - eAR(n,p) \tag{18}$$

which can be solved by the standard form

$$\frac{dy}{dx} + py = Q \tag{19}$$

$$y = \left[\int_0^x Q \exp\left(\int_0^x p\,dx'\right) dx + c \right] / \exp\left(\int_0^x p\,dx'\right) \tag{20}$$

The result is

$$I_p(d) = \frac{\left(\int_0^d \left|\left[\alpha I - eAR(n,p)\right] \exp \int_0^x P\,dx'\right| dx + I_p(o)\right)}{\exp \int_0^d P\,dx} \tag{21}$$

where $P = (\alpha-\beta)$, the difference between the hole and electron avalanche ionization coefficient d is the thickness of the depletion region, and $I_p(o)$ is the saturation current of holes incident from the n-side of the p-n junction.

Equation 21 cannot be integrated directly because the avalanche coefficients are very complicated functions of position within the depletion region.

The shape of the avalanche ionization coefficient curves, as a function of position, can take on different forms, depending on the doping concentration and the geometry of the device. One particular form obtained from the work of Overstraeten and Deran (Ref. 15) is shown in Figure 2. To make the calculation as simple as possible, use average values for these coefficients; call them $\bar{\alpha}$ and $\bar{\beta}$. Making these approximations and ignoring the generation-recombination term, we obtain the current for a p-n junction device operating in the avalanche region by integrating Equation 21.

$$I_p(d) = I_p(o) \exp(-\bar{p}d) + \frac{\bar{\alpha}}{\bar{p}} [1 - \exp(-\bar{p}d)]I \tag{22}$$

where $\bar{p} = (\bar{\alpha}-\bar{\beta})$.

Now if Sze's approximation is used (Ref. 14), (i.e., $I = I_p(d) + I_n(d) \approx I_p(d)$), the following form is obtained.

$$I \quad \frac{I_p(o)(\bar{\beta}-\bar{\alpha})e^{(\bar{\beta}-\bar{\alpha})d}}{\left[\bar{\beta}-\bar{\alpha}\, e^{(\bar{\beta}-\bar{\alpha})d}\right]} \tag{23}$$

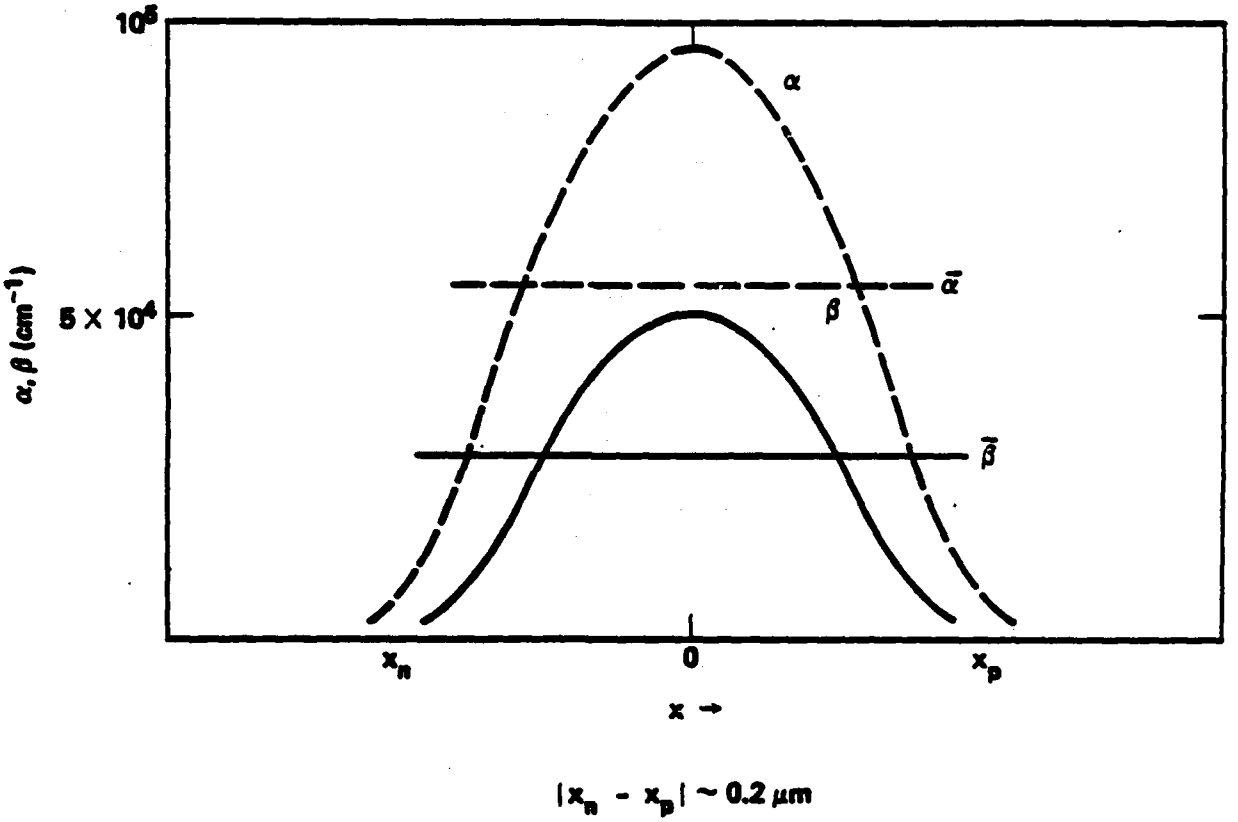

Figure 2. Ionization coefficients for electrons and holes in some typical p-n junction diodes.

Equation 23 has the exact same form as the current in a Townsend discharge in gases in the avalanche region (Ref. 16). That is

$$i = \frac{i_o(\alpha-\beta)d^{(\alpha-\beta)d}}{\left[\alpha - \beta e^{(\alpha-\beta)d}\right]} \tag{24}$$

where α and $\gamma = \beta/\alpha$ are the electron and positive ion ionization coefficients (Ref. 16) in a gas discharge device.

Note that Equation 23 is not exact, but an approximate solution to Equations 4 through 9.

For the reverse-bias case in which the generation-recombination is not neglected, we obtain, after integration of Equation 21, the current as follows:

$$I = \frac{I_p(o)\ \tau_e \bar{p}\ \exp(\bar{-}pd) + n_i eA[1 - \exp(-\bar{p}d)]}{\tau\bar{p}\left\{1 - \frac{\bar{\alpha}}{\bar{p}}\ [1 - \exp(-\bar{p}d)]\right\}} \tag{25}$$

The saturation current $I_p(o)$ is (Ref. 17):

$$I_p(o) = e\left(\frac{D_p}{\pi}\right)^{1/2}\ \frac{n_i^2}{N_d}\ A \tag{26}$$

where D_p is the diffusion coefficient for holes, and N_d is the donor doping concentration in the n-side.

Starting with a one-dimensional form of Equation 9 where we have approximated heat loss in the other two dimensions with a thermal conductance λ, we get (Ref. 17):

$$pc\ \frac{dT}{dt} = JE + \frac{\partial}{\partial x}\ (K(x,t)\ \frac{\partial T}{\partial x}) - \lambda(T-T_o) \tag{27}$$

For the steady-state case ($\frac{\partial T}{\partial t} = o$) with no variation of T with x, this equation becomes:

$$JE = \lambda(T-T_o) \tag{28}$$

Using Equations 25, 26, and 28, and the data in Figure 3, we obtain the approximate I vs. V curve shown in Figure 3.

Figure 3 shows that Equation 25, together with Equation 26, does give rise to a negative resistance region similar to that in a gas discharge device when thermionic emission has set in.

Again, Equation 25 is only an approximate solution of Equations 4 through 9.

We can draw an analogy with the breakdown region in a gas discharge and second breakdown in a p-n junction device. In a gas discharge, the physical phenomenon which gives rise to breakdown is the thermionic emission of electrons from the cathode. In a p-n junction device, the physical phenomenon which gives rise to second breakdown is the thermal excitation of electrons from the valence bands. Physically speaking, the two processes are very much the same, as shown in Figure 4. In a gas discharge, it is the potential barrier at the surface that governs the emission of the electrons; in a solid, it is the band-gap of the semiconductor which governs thermal emission of the electrons from the valence bands.

Another simple model which can be used to explain the physical mechanisms of second breakdown is based upon the fact that, when a device is operating in the second breakdown mode, the free carriers generated are primarily due to thermal excitation of the electrons from the valence bands. Therefore, for high temperature and low doping concentration (e.g., below $10^{15}/cm^3$) (Ref. 18), the current density can be approximately written as follows:

$$J \cong v_n q n_i + v_p q n_i$$

where v_n and v_p are drift velocities of the electrons and holes, and the intrinsic carrier concentration n_i is (Ref. 14):

$$n_i = 2\left(\frac{2\pi m_o K}{h^2}\right)^{3/2} \left(\frac{m_e m_h}{m_o^2}\right)^{3/4} T^{3/2} \exp\left(\frac{E_g}{2KT}\right) \qquad (16)$$

where

E_g = forbidden gap energy

K = Boltzmann's constant

h = Planck's constant

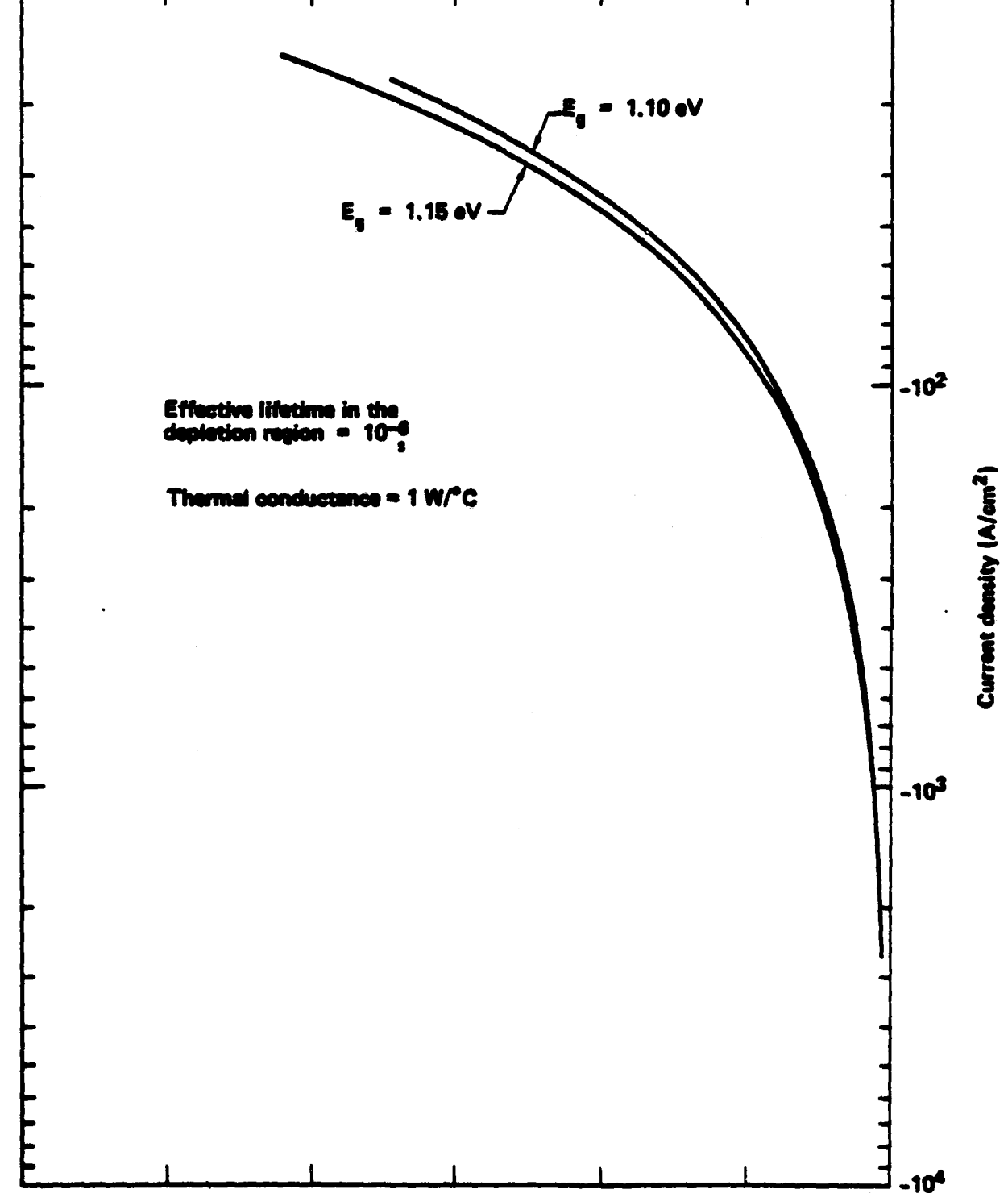

Figure 3. I-V characteristics in the second breakdown region of a p-n junction based on thermal excitation models.

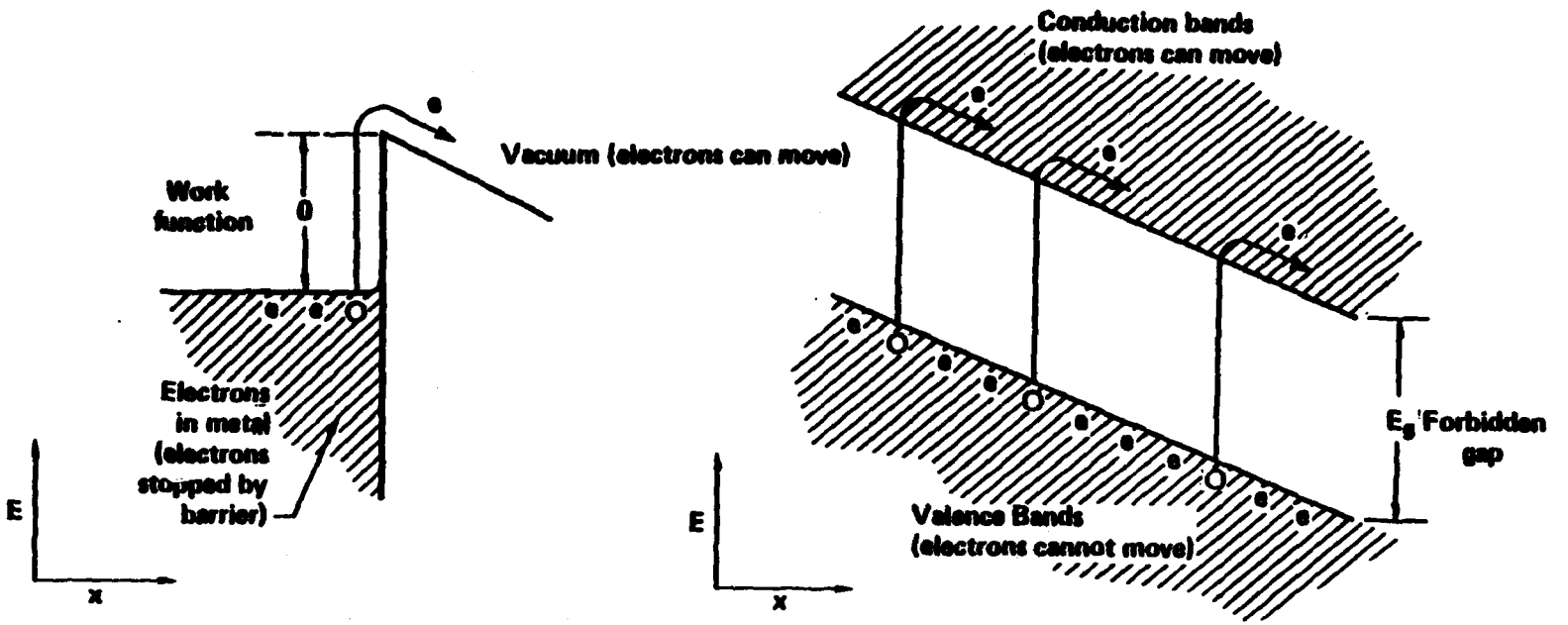

Figure 4. Energy band diagrams showing the similarity between thermionic emission of electrons out of a metal and thermal excitation of electrons out of the valence bands in a semiconductor.

The electron and hole effective masses m_e and m_h which appear in Equation 30 are, in general, a function of the temperature and the electric field. This is because the band structure of a material changes with the application of high temperatures and high electric fields. However, for a simple analysis, assume that the effective masses are constant.

In the avalanching region, the drift velocities v_n and v_p will be scattering limited. For an electric field above 3.5×10^5 V/cm, the velocity can be approximated by (Ref. 19):

$$v_n(\text{cm/s}) = 1.45 \times 10^6 \, E^{0.1525} \tag{31}$$

$$v_p(\text{cm/s}) = 4.68 \times 10^4 \, E^{0.4445} \tag{32}$$

where E (V/cm) is the electric field in the semiconductor. In a real situation, the velocity is not just a function of the electrical field but also a function of temperature (Ref. 20). Assume a simple one-dimensional model with an n^+-Intrinsic-n^+ configuration in series with a fixed resistor and voltage source. If we assume that the thermal conductivity (K) is independent of position and that steady state conditions prevail, then Equation 27 reduces to:

$$K \frac{\partial^2 T}{\partial x^2} = \lambda(T-T_o) - JE \tag{33}$$

This geometry and equation are similar to those used by Shousha (Ref. 21) in his investigation of second breakdown in insulated thin films.

Using Equations 29 to 32, and solving Equation 33 numerically, we obtain the I versus V curve and the spatial distribution of the temperature. Note that the results shown in Figure 5 are quite similar to those obtained by Shousha (Ref. 21) for thin films. The fact that a simple system like that given above exhibits negative resistance also supports the experimental fact that second breakdown phenomena can occur, not only in junction devices, but also in homogeneous materials. From Figure 5, you can see that, as the current increases, a hot spot forms at the center of the device.

Another experimental fact which seems to support the model proposed here is the relatively good agreement between the measured resistivity curve and the theoretical resistivity from Equation 29 (Fig. 6).

Up to now, only steady-state operation of a device has been considered. The next step in the complexity of the model is to consider the time-dependent form of the transport equation. This is because, once a device gets into the second breakdown region, the physics is very nonstationary. As a first attempt to more accurately characterize the effects of second breakdown, we have

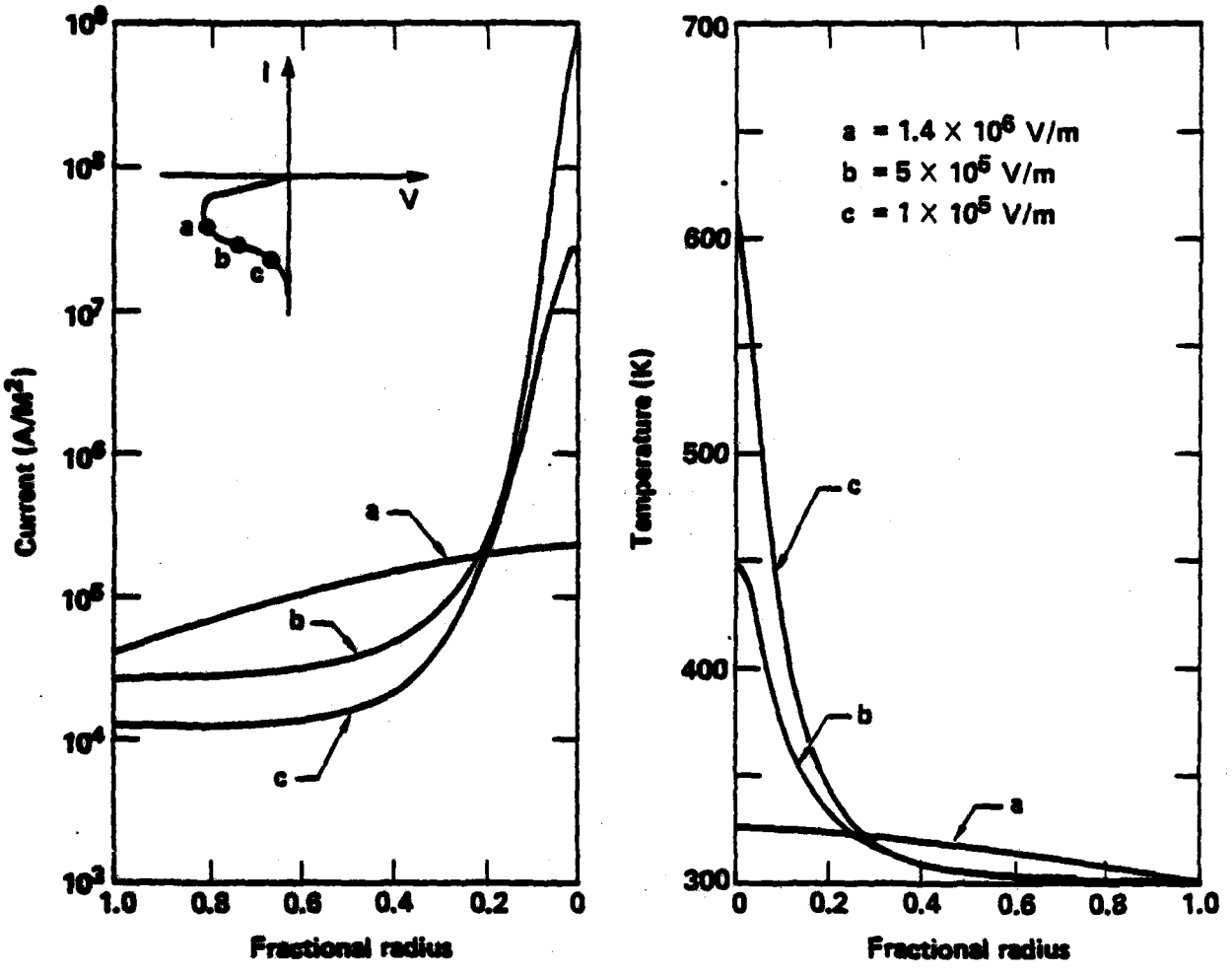

Figure 5. Steady state current density and temperature as a function of radius in a cylindrical junction at three points in the second breakdown region. ("0" is at the center of the device and "1" is at the edge.)

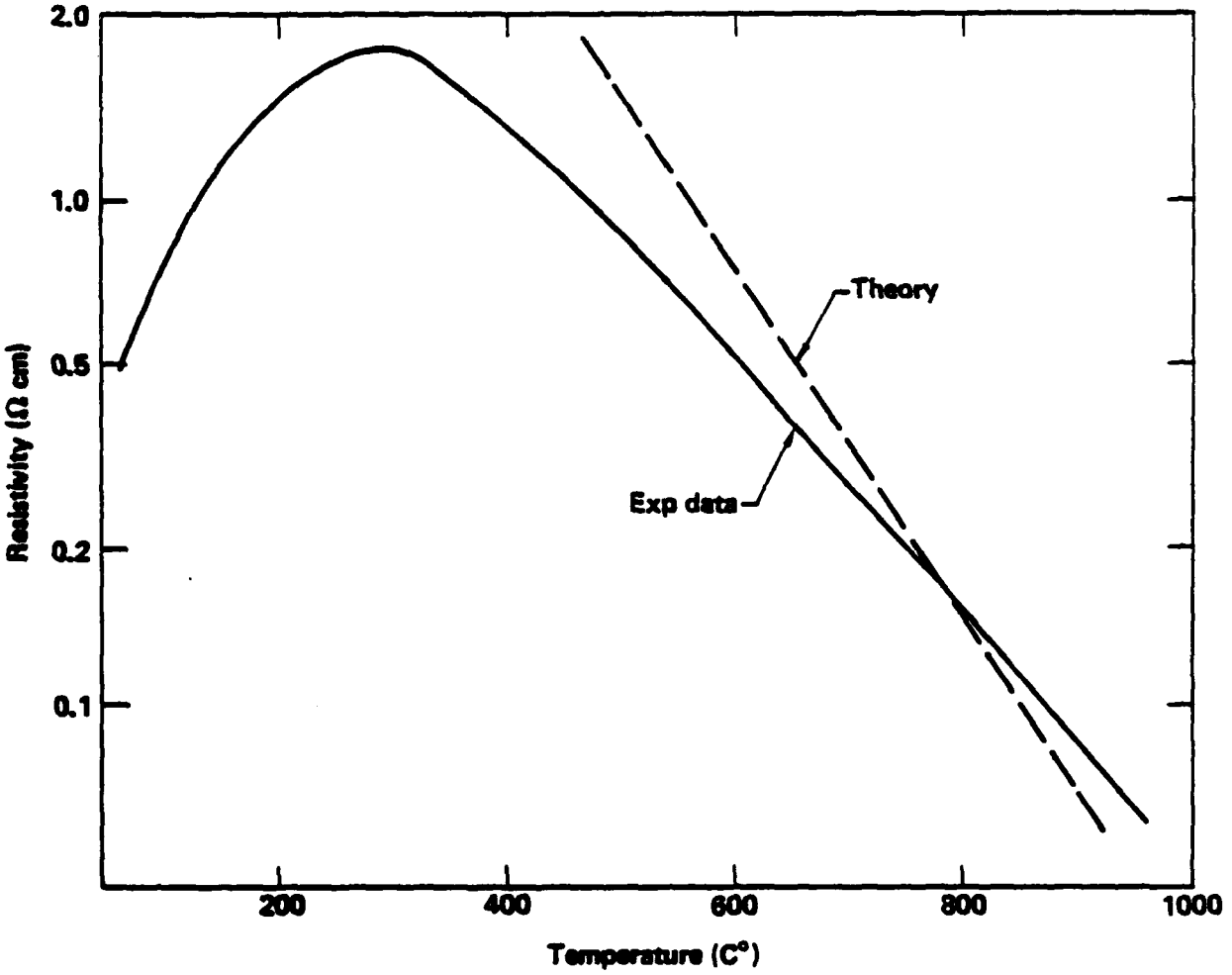

Figure 6. Comparison between the experimental and the theoretical resistivity data.

created a cylindrical, two-dimensional, time-dependent model for a junction device operating in a high field situation. The device configuration is a thin silicon disk imbedded in a silicon substrate, with noninjecting contacts on the top and bottom (Fig. 7). The device is in a series circuit with a voltage source and a load resistor. Second-breakdown phenomena in this device are investigated by solving the nonlinear transport equations for electrons and holes, together with the time dependent thermal energy transport equation.

To solve the thermal and electronic transport equations, we first assume that the device is thin enough to allow us to ignore variations of parameters along the axis of the cylinder. These parameters include the electric field, temperature, avalanche coefficients, and thermal conductivites. The temperature at any point in the radial direction is determined by solving the thermal diffusion equation

$$\rho C \left(\frac{\partial T}{\partial t}\right) = \nabla_r (K \nabla_r T) + JE - \left(\frac{\lambda}{d}\right) (T - T_o) \tag{34}$$

where ∇_r is the radial component of the gradient, K is the thermal conductivity, λ is a thermal conductance, d is the thickness of the device, ρ is the density, and C is the heat capacity. Radial heat flow is determined by the first term on the right-hand side. The second term on the right-hand side is just the ohmic heating in the device, and the third term is the heat flow along the axis of the device. This equation is solved using a finite difference method.

The current density is calculated from the charge carrier density and the drift velocity.

$$J = nev_n + pev_p \tag{35}$$

where e is the magnitude of an elementary charge. The drift velocity as a function of the field uses Equations 31 and 32 for high fields and standard mobility equations for low fields, and the charge carrier density is determined by solving the continuity equation (ignoring electronic diffusion)

$$\left(\frac{\partial n}{\partial t}\right) = G(E,T) - U(T) \tag{36}$$

where G is the avalanche generation rate and U is the intrinsic thermal recombination (generation) rate. All of these equations are solved simultaneously with the circuit equation,

$$V = IR + V_o \tag{37}$$

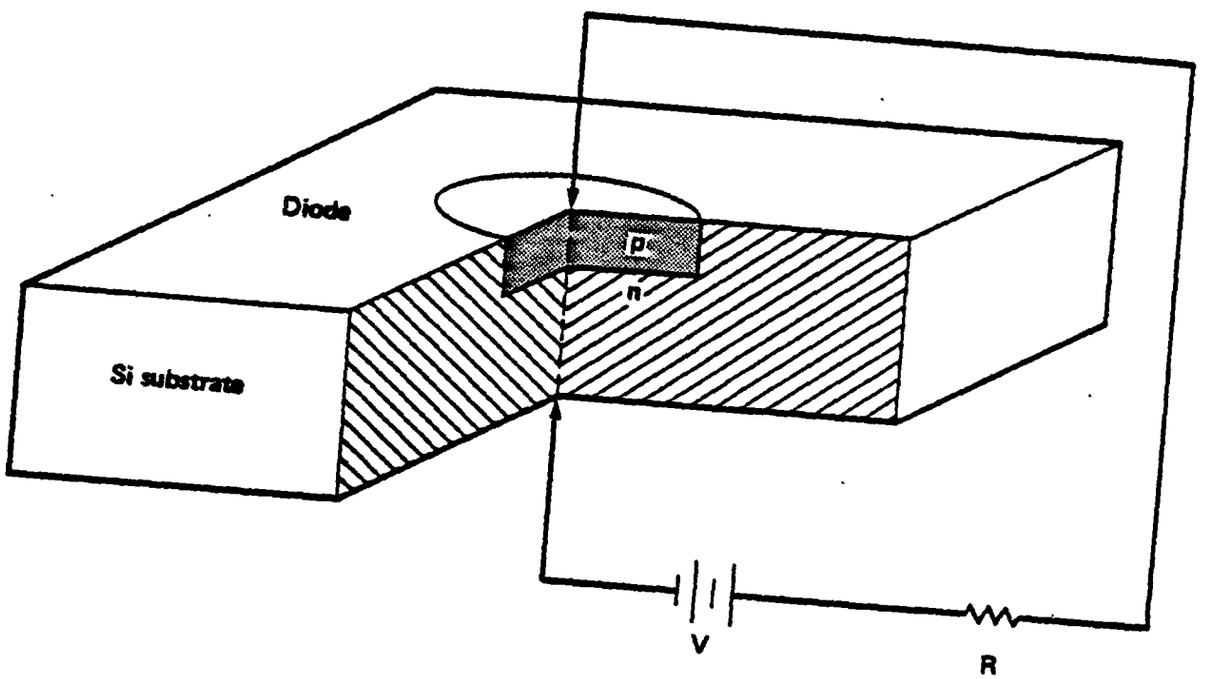

Figure 7. Configuration of the cylindrical p-n junction used for this analysis.

where V and R are the applied voltage and load resistance, I is the total current, and V_0 is the voltage across the device.

The results of these calculations are displayed as plots of current and voltage versus time, and current density and temperature versus position. From the current and voltage plots, you can determine the failure threshold power and the power duration to failure for the device in different internal and external environments.

Avalanche breakdown (A) and the subsequent heating and thermal second breakdown (B) are readily apparent from the plots of current and voltage (Fig. 8). Hot spot formation is evident in the plot of temperature versus radial distance (Fig. 9). Each line on this plot represents the temperature or current density at a particular time step (1×10^{-4} s). Note how the device first heats up evenly under a uniform current density. When a critical temperature has been reached (between 600 and 800 K), the current density and temperature collapse into a current filament and a hot spot.

As it stands, this model of device operation is a relatively fast method of comparing sensitivites of thermal second breakdown power levels and times to the various device parameters. Also, it seems to be giving more insight into the mechanisms and operation of devices in the second breakdown regime. Plans are to extend this model to three dimensions in a cylindrical geometry and two or three dimensions in a rectangular geometry. When this is realized, more complex geometries can be considered and the effects of current mode second breakdown included.

CURRENT MODE SECOND BREAKDOWN

If the pulse width of an applied voltage is in the microsecond range or longer, the shape of the threshold failure power curve obtained from some experimental investigations approximately follows the WB model. As the width of the pulse gets shorter, say about 10 ns, the shape and the magnitude of the threshold failure power curve no longer follows the WB model (Ref. 22). At the present time, there are no theoretical models that explain this discrepancy, although it has been observed that, when a breakdown occurs near the surface or contacts of a device, the threshold failure power of the device is much smaller than that predicted by the WB model. The reason that the WB model cannot explain this observation may be due to the fact that the physics of second breakdown induced by a short pulse is quite different from the thermal breakdown described by the WB model.

In the short pulse range, especially in bipolar transistors there often occurs another second breakdown phenomenon called "Current Mode Second Breakdown." Current mode second breakdown is quite different from the thermal second breakdown (Ref. 23). The delay time for the current mode breakdown is on the order of a nanosecond. On the other hand, the delay time for thermal second breakdown is on the order of microseconds or longer. Physically, current mode breakdown is induced by an electronic (Ref. 22) rather than a thermal process.

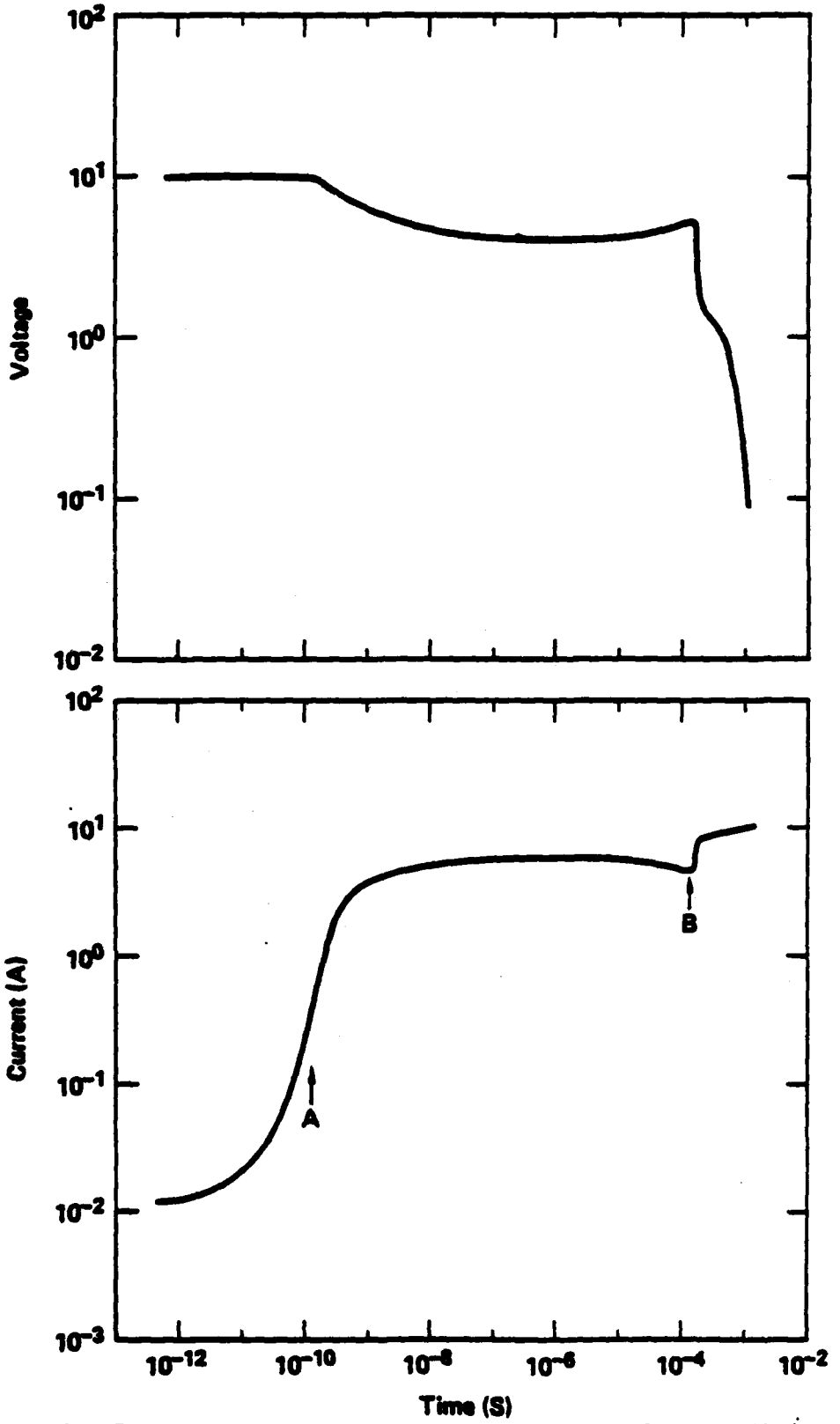

Figure 8. Time history of the voltage and current for the diode simulation. (Note, avalanche (A) and thermal (B) breakdown.)

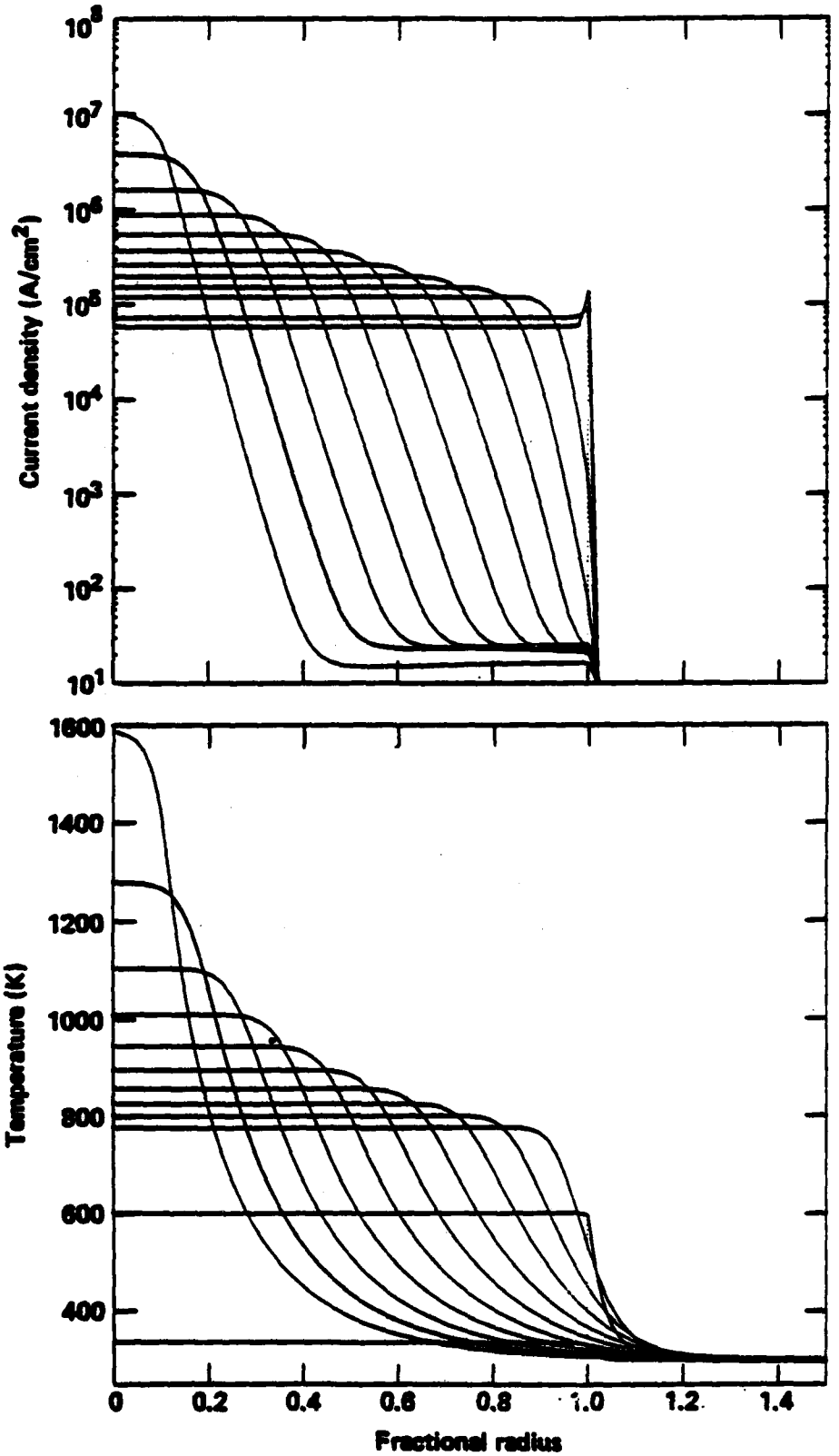

Figure 9. Current density and temperature during thermal and avalanche breakdown for the diode model. (Each line is for one time step of 1×10^{-4} s.)

Recently, Keiichi, et al. (Ref. 22), have investigated current mode breakdown theoretically by solving part of the continuity equations together with the heat flow equations. The results obtained from their calculations show that you can switch between current mode second breakdown and thermal second breakdown by changing either the applied collector voltage or the external load resistance (see Fig. 10). Now, since the delay time for the current mode breakdown is on the order of a nanosecond, it is possible that the experimental observations of breakdown phenomena with nanosecond delay time were due to current mode second breakdown rather than to thermal second breakdown. If the breakdown phenomena which occur in the short pulse ranges are indeed due to current mode breakdown, then you would not expect the WB model to agree with the experimental results. Therefore, theoretical investigations into the current mode breakdown are important to the understanding of EMP burnout phenomena.

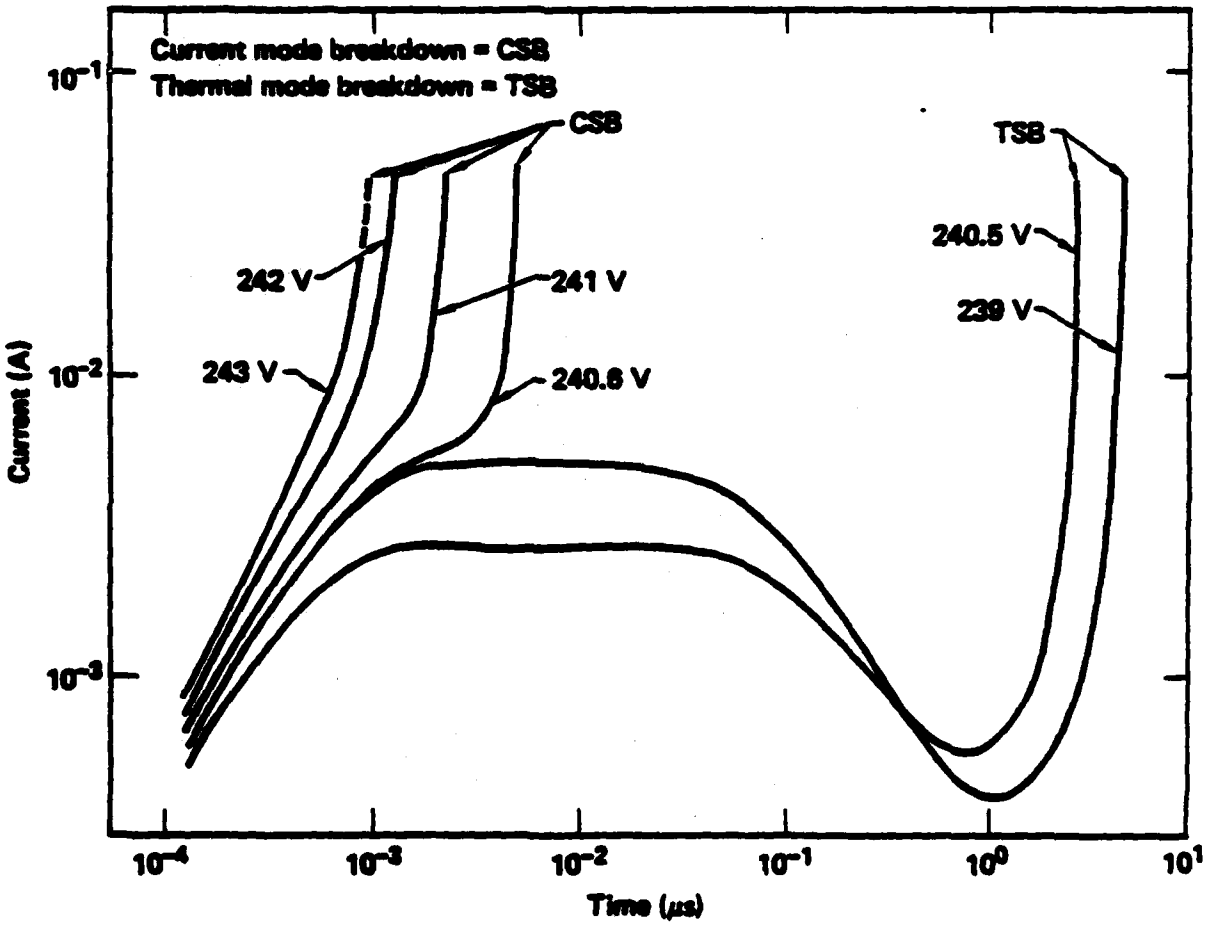

Figure 10. Variation of total current I versus time as a function of terminal voltage V for the current mode and thermal mode second breakdown.

MULTIPLE HOT SPOT FORMATIONS AND THEIR EFFECT ON THE TRANSPORT PARAMETERS OF THE DEVICES

Hot spots caused by high localized temperatures can be very damaging to a device's electron and hole transport properties. This is because the temperature in the hot spots can reach the melting point of the material. When this happens, the mechanical damage caused by the hot spots induce many localized energy levels in the band-gap of the semiconductor. After a device has been subjected to localized hot spot formation, the transport properties of the device may be different. For example, if the diffusion lengths and the minority lifetime are measured (at room temperature) after the device has been subjected to the hot spot formation, both may be shortened. The doping concentration in the regions where hot spots occurred may also be changed. This also alters the transport properties of the device.

Note that the lifetime of the free carriers may actually be longer during the time when the temperature of the device was high. This is because, at high temperatures, more free carriers are released from deep traps in the crystal than are being captured. In other words, the capture probability of a free carrier is smaller than the emission probability.

If damage occurs in the depletion region of the device, the recombination current will increase, which increases the dark current of the device. This changes the shape of the I versus V curve. This is what happens experimentally when a device operates in the second breakdown region for a long time.

Up to now, there has been no explanation for quantitative or qualitative multiple spot formations in the second breakdown region. However, based upon the following reasoning, you can see how multiple hot spots could be formed qualitatively. Assume that the hot spot of a device is formed at point A (on Fig. 11). Now since the temperature of the hot spot is much higher than its surroundings, the thermal expansion of the hot spot exerts a stress in the region. As a result, the band-gap of the surrounding regions increases, as shown in Figure 11. Consequently, more current flows through the hot spot and through point B, than in the surrounding regions. Once this happens, another hot spot will form at point B. The thermal stress created at point B now causes the band-gap of its surrounding material to increase. Another hot spot will then be formed at point C.

To put the physics quantitatively, or to model multiple hot spot formations as described, a relationship between the nonuniform thermal stress and its effect on a device's band-gap must be found.

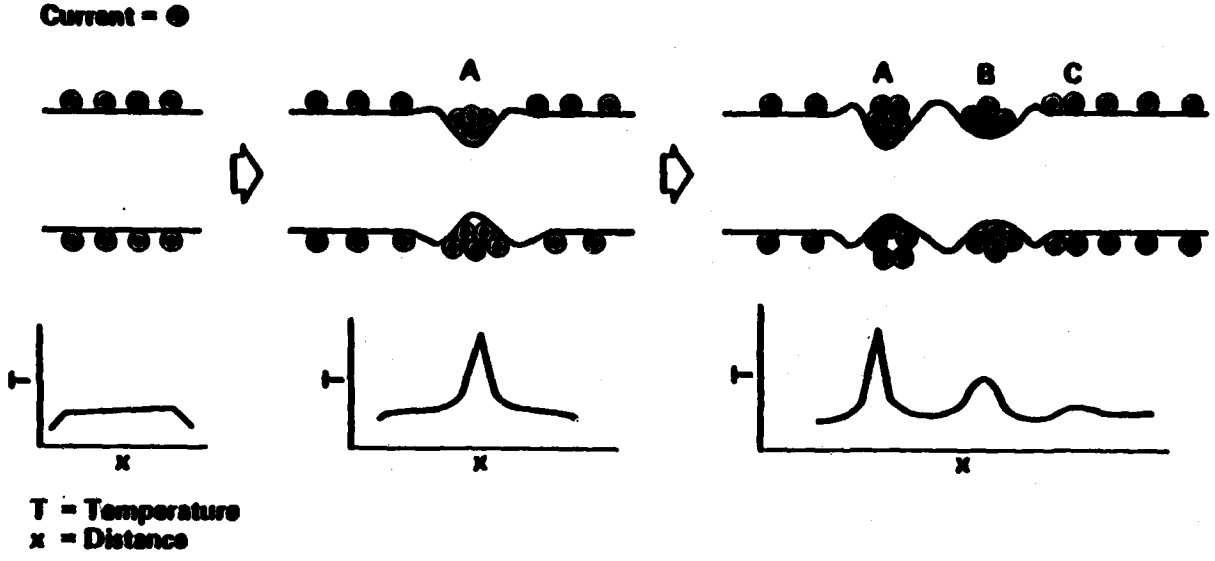

Figure 11. Explanation of the multiple hot spot formations by the distortions of the energy bands.

SOME RECENT EXPERIMENTAL RESULTS

The lack of theoretical progress in the understanding of the complex physical phenomena of second breakdown makes it difficult to predict accurately the threshold failure power of junction devices. As a result, the tendency of most recent experimental work is to test as many devices as possible to try to check for any kind of universal failure distribution. For example, BDM Corporation recently tested 10,000 bipolar transistors (Ref. 23). The objective of the work was to examine a sufficiently large number of commercially available devices to permit statistically significant statements to be made concerning the functional form and the parametric values of the failure distributions. Furthermore, sufficient experimental controls were required to provide a basis for extrapolating the results to device types not specifically included in the experimental effort. No universal failure distribution was found, however. Instead, the tests showed that the failure threshold distributions were different for different device configurations. In some cases, even the same cell configuration gave different results when the devices were made from different wafers. Nevertheless, the investigation provided some useful conclusions. They are: (1) periphery is a better predictor of emitter-base failure threshold than total area; (2) the emitter-base may be the most vulnerable junction to failure even when electrical overstress is applied to the collector; and (3) gold doping tends to degrade the failure threshold for the emitter-base configuration.

In addition to the BDM work, Bruno Kalab has carried out extensive investigations into the junction burnout phenomena in transistors and diode devices (Ref. 5). The conclusions from his work can be summarized as follows: (1) the failure mechanisms of semiconductor devices are not yet understood; (2) it is difficult, if not impossible, to fit the experimental data to the WB model, especially in the short pulse width pulse region in the threshold failure curve; and (3) other unknown breakdown phenomena occur in the short time delay region.

Although both the BDM and Bruno Kalab's work are quite extensive experimentally, they do not provide any definite information concerning the failure mechanisms of semiconductor junction devices. However, you can still draw some useful information concerning procurement practices from their work. These are: (1) avoid sharp corners in the topological layout; (2) obtain, if possible, all devices of one kind from a single manufacturer; and (3) avoid doping with Au or other metal impurities (Cu, Ag, etc.)

OTHER DAMAGE MECHANISMS

PULSE CURRENT DAMAGE TO MOS DEVICES

Unique to MOS is an oxide layer which serves as an insulator between the metalization and doped silicon. The conductivity of the silicon is modulated by the field developed across the oxide due to an applied voltage at the metalization. The failure mode associated with the oxide layer is oxide breakdown.

The failure mode associated with the oxide layer arises from voids and inhomogeneities within the oxide. The physical mechanisms which cause the breakdown can be explained with the following theoretical consideration (Ref. 24). In general, voids which occur within the oxide or dielectrics can have many different shapes and sizes. However, for the simplicity of theoretical calulations, assume that the voids have, on the average, a form like that shown in Figure 12. With this assumption, it can be shown, by solving Laplace's equation, that the field around the void takes the following form (Ref. 24):

$$\bar{E}(r,\theta) = \left\{ E_0 \cos\theta \left[2 \cdot \left(\frac{1 - \epsilon_M}{1 + 2\epsilon_M} \right) \frac{a^3}{r^3} + 1 \right] \right\} \bar{r} + \left\{ E_0 \sin\theta \left[\left(\frac{1 - \epsilon_M}{1 + 2\epsilon_M} \right) \frac{a^3}{r^3} - 1 \right] \right\} \bar{\theta} \tag{38}$$

where E_0 is the applied field and E_m is the dielectric constant. The maximum field compression is at $\theta^0 = -\pi/2$ and $r = a$.

$$\bar{E}\left(r = a, \theta = -\frac{\pi}{2}\right) = -E_0 \left[\frac{1 - \epsilon_M}{1 + 2\epsilon_M} - 1 \right] \bar{\theta} \tag{39}$$

$$\bar{E} = \frac{4}{3} \bar{E}_0 (\epsilon_M = 4)$$

Therefore, for points near the void ($r \cong a$), the field is enhanced by a factor of 4/3. Thus, for a thin layer, the field required to produce oxide breakdown is only 3/4 of that predicted by the model for the homogeneous oxide.

ELECTROMIGRATION

Electromigration is a term applied to the transport of mass in metals when the metals are stressed at high current densities. This effect has been known for several decades and has been observed in both molten and solid

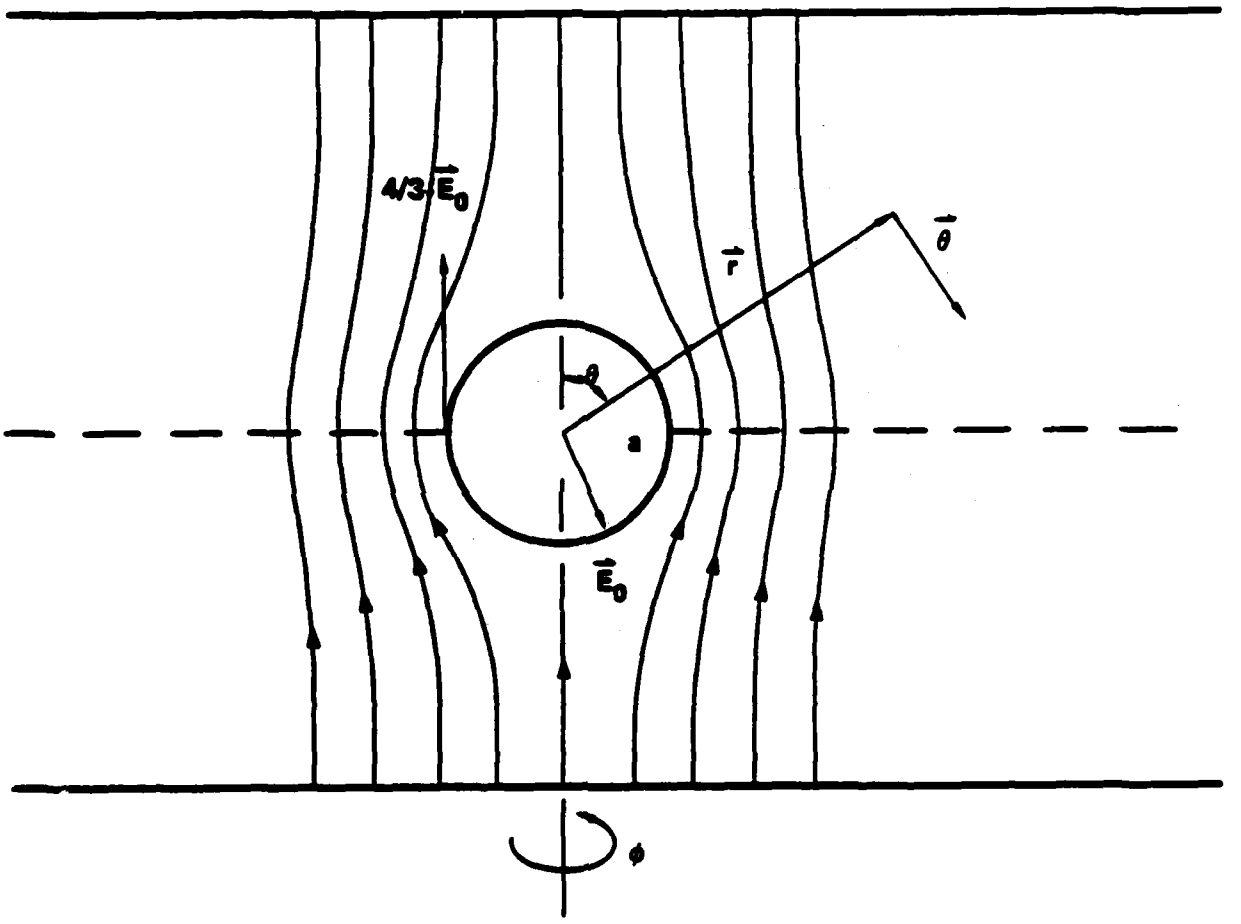

Figure 12. Defect model used in calculating the electic field near the voids.

metals (Ref. 25). Recently, electromigration has been recognized as a potential wear-out failure mode in semiconductor devices employing metal film conductors of inadequate cross-sectional area, and has stimulated investigations of mass transport in metal films. The failure is an electrical open circuit due to the apparent loss of conductor metal.

The damage mechanism electromigration can also cause the contact to break off from the devices if the contact is not properly made. The break-off of the contact under high current due to the migration of the masses also results in open circuits.

ELECTRICAL BREAKDOWN BETWEEN METALIZATION STRIPS

When the electrical field between two etched conducting paths on the semiconductor or insulator wafer exceeds the breakdown limit of the intervening materials, the result can be an arc which can short the strips together by forming a channel from the melted metal. The result can be a short circuit for the device or the circuit. This is illustrated in Figure 13.

The metalization strip breakdown mechanism will become more important as feature sizes in integrated circuits continue to decrease, implying that even small voltages will suffice to create enormous electric fields within the devices. Coupled with the fact that smaller junctions are more easily damaged thermally, it seems clear that future semiconductor devices used in military systems will be even more vulnerable to electrical stress damage than those in use today.

HIGH FIELD SURFACE BREAKDOWN

The surface conditions of a p-n junction influence the electrical characteristics of the devices (Ref. 26) because the surface recombination process, which depends on the surface conditions, acts as a sink for free carriers. The surface of a device can be damaged mechanically or electrically. One of the causes of surface damage is high surface field breakdown. For semiconductor devices, this high electric field occurs near the space charge layer on the surface. For an ideal surface, the field distribution on the surface can be controlled by proper design of the device geometry. Daves and Gentry (Ref. 26) have shown that this is the case by solving Poisson's equation. For a surface of unknown nature, however, there exists no general theory as to how the field on the surface can be reduced. High field at the surface not only can cause surface breakdown, but also can cause the migration of the ionized surface impurities. Therefore, by reducing the field at the surface, you can also reduce the probability of migration of the ions, thus making the device more stable.

Another problem which causes surface breakdown is surface tracking caused by the deposition of metal dust on the surface. The metal dust sometimes acts like a metal film which can cause shorts in the devices. When two metal dust particles are close by, they can create high localized fields like two metal strips. As a result, surface breakdown can occur. In general, there are other mechanisms which can also cause surface breakdown, such as breaking bonds of atoms at the surface with high fields. This often occurs in organic dielectrics (Ref. 27).

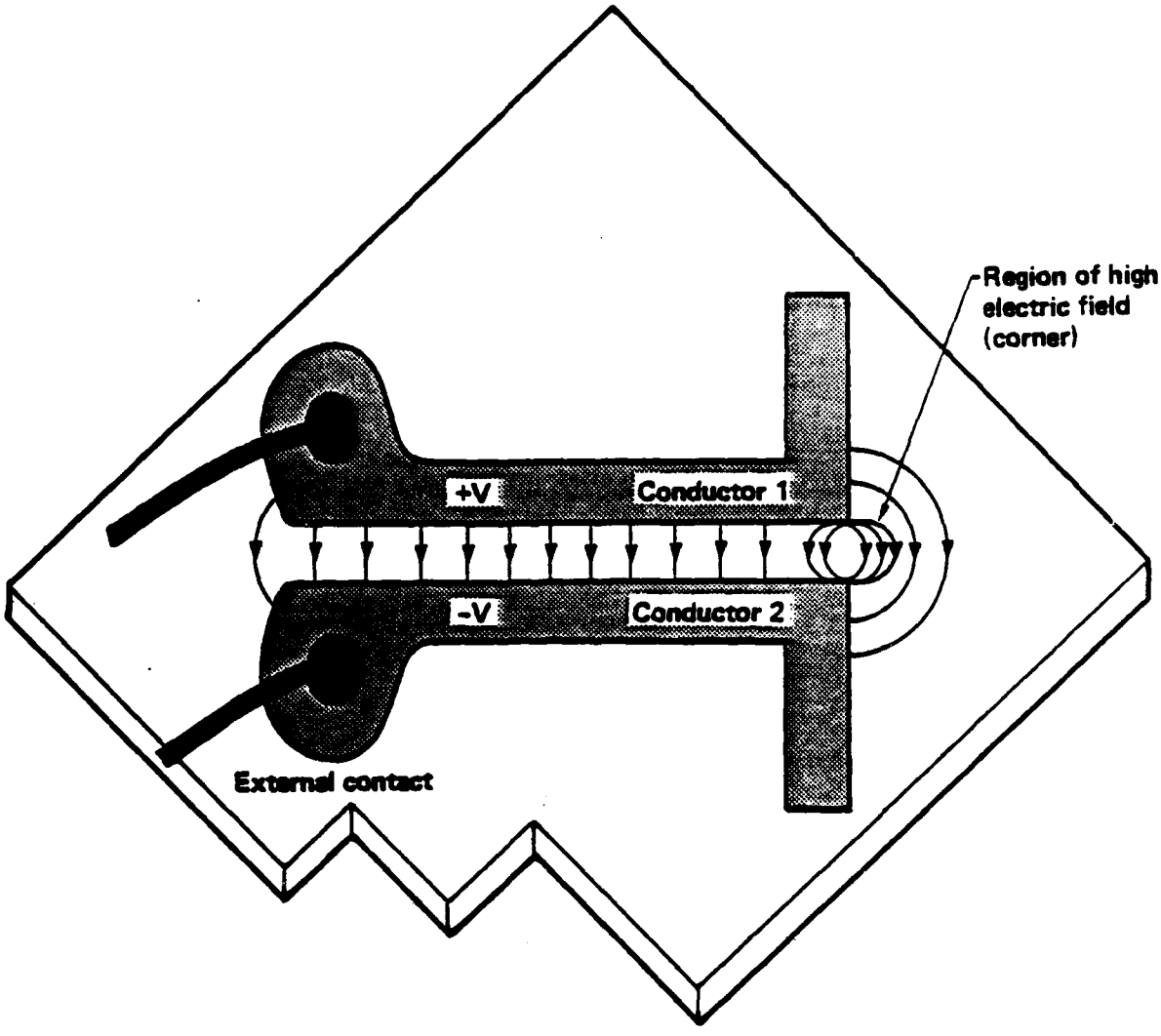

a. Corners (Top View)

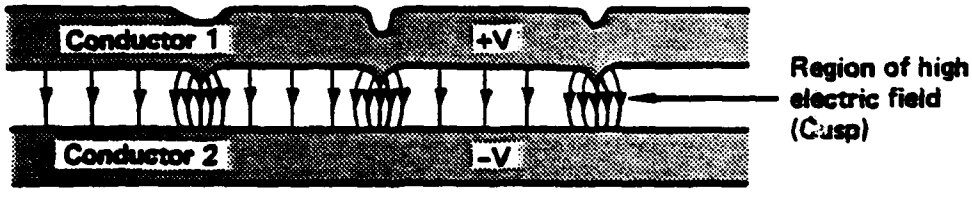

b. Cusps (Side View)

Figure 13. Metallization strips voltage breakdown.

CONCLUSION

Many models have been proposed to investigate the second breakdown phenomenon. Because of the complexity of this phenomenon, most of the existing models do not accurately describe it. Many assumptions were made in these models. For this reason, the theoretical results obtained from the calculations based on these models do not agree well with the experimental results. Ward's model appears to be the most basic and correct (Ref. 7); however, he simplified the problem by treating it in only one dimension. In addition, he took his calculation up to only 600 K. In principle, Ward's model should adequately describe the physical phenomena, including the hot spot formation, if the physical parameters which occur in the equations are accurately known, and if the calculation is extended to two or three dimensions and to higher temperatures.

One of the most difficult problems now facing the EMP device theorists is finding a way to explain the variations in the experimental data for threshold failure power as a function of pulse width, and the variation in the failure probability distribution function as a function of the failure power. The existing data show that the threshold failure power for a set of identical devices can vary as much as two orders of magnitude in the failure power-pulse width curve. The uncertainty is too wide for the predictability of the threshold power based on the existing data.

There are many parameters which can influence the variation of the threshold failure power. These are doping density, inhomogeneity, vacancies, dislocations, surface conditions, and the geometric dimensions of the devices. Therefore, in order to narrow down the variations of the threshold power for a given set of devices, all of these parameters must be considered.

After going through various calculations in our work, we believe that we have come a little closer to understanding the physical mechanisms of second breakdown than before. However, in order to understand why the WB model does not agree with the experimental result, especially in the short pulse region, the complete set of device equations need to be solved. That set includes the continuity equation, Poisson's equation, and the thermal transport equation, because, when the pulse width of the applied voltage (or current) is short, the second breakdown phenomena may be due to current mode breakdown.

REFERENCES

1. Wunsch, D. C. and R. R. Bell, "Determination of Threshold Failure Levels of Semiconductor Diodes and Transistors Due to Pulse Power Voltages," IEEE Transactions on Nuclear Science, Vol. NS-15, No. 6, December 1968.

2. Bedrosian, G., R. Christie and V. Tatoian, A Critical Review of Semiconductor Failure Modeling for Nuclear Hardening, The Dikewood Corporation, Albuquerque, New Mexico, September 26, 1980.

3. Electronic Component Modeling and Testing Program, Pt. 1, AFWL-TR-78-62, Air Force Weapons Laboratory, KAFB, New Mexico, March 1980.

4. Grutchfield, H. B. and T. J. Moutoux, "Current Mode Second Breakdown in Epitaxial Planar Transistors," IEEE Transaction of Electron Devices, Vol. ED-13, No. 11, p. 743 (1966).

5. Kalab, Bruno M., Damage Characterization of Semiconductor Devices for the AN/TRC-145 EMP Study, Harry Diamond Laboratories, Adelphi, Maryland, HDL-TR-1915, December 1980.

6. Kleiner, C., et al., "Integrated Circuit Model Development for EMP," IEEE Transactions on Nuclear Science, Vol. NS-21, p. 323 (1974).

7. Ward, A. L., "Doping Profiles and Second Breakdown," Electrical Overstress/Electrostatic Discharge Symposium Proceedings, EOS-1, Denver, Colorado, p. 109 (1979).

8. Tasca, D. M., J. C. Peden and J. Miletta, "Non-Destructive Screening for Second Breakdown," IEEE Transactions on Nuclear Science, NS-19, pp. 57-67, December 1972.

9. Barush, A. and P. P. Budenstein, "An Electrothermal Model for Current Filamentation in Second Breakdown of Silicon on Sapphire Diodes," Electrical Overstress/Electrostatic Discharge Symposium Proceedings, EOS-1, Denver, Colorado, p. 126 (1979).

10. Kusnezov, N., and J. S. Smith, "Modeling of Electrical Overstress in Silicon Devices," Electrical Overstress/Electrostatic Discharge Symposium Proceedings, EOS-1, Denver, Colorado, p. 133 (1979).

11. Hower, P. L., et al., "Stable Hot Spots and Second Breakdown in Power Transistors," PESC 76 Record, 1976 IEEE Power Electronics Specialists Conference, Cleveland, Ohio, June 1976.

12. Scarlett, R. M. and W. Shockley, "Secondary Breakdown and Hot Spots in Power Transistors," 1963 IEEE International Convention Record, Pt. 3, pp. 3-13.

13. Hower, P. L. and P. K. Govil, "Comparison of One- and Two-Dimensional Models of Transistor Thermal Instability," IEEE Transactions on Electron Devices, Vol. ED-21, No. 10, p. 617 (1974).

14. Sze, S. M., Physics of Semiconductor Devices, Wiley-Interscience, 1969.

15. Van Overstraeten, R. and H. De Man, "Measurement of the Ionization Rates in Diffused Silicon p-n Junctions," Solid State Electronics, Vol. 13, pp. 583-608 (1970).

16. Loeb, L. B., Fundamental Processes of Electrical Discharge in Gases, John Wiley & Sons, Inc., London: Chapman & Hall, Limited, p. 378 (1939).

17. Raburn, W. D. and W. H. Causey, Determination of Semiconductor Junction Vulnerability to Second Breakdown, U.S. Army Missile Research and Development Command, Redstone Arsenal, Alabama, EA-CR-77-1 (1977).

18. Budenstein, Paul P., et al., Second Breakdown and Damage in Semiconductor Junction Devices, U.S. Army Missile Command, Redstone Arsenal, Alabama, RG-TR-72-15, April 1972.

19. Bowers, H. C., "Space Charge Induced Megative Resistance in Avalanche Diodes," IEEE Trans. Elect. Dev., ED-15, No. 6 (1968).

20. Lanyon, H. P. D., "Electron Transport and Ionization in Silicon at High Fields," Solid State Electron, Vol. 21, p. 291 (1978).

21. Shousha, A. H. M., "Negative Differential Conductivity Due to Electrothermal Instabilities in Thin Amorphous Films," J. Appl. Phys., Vol. 42, No. 12, 5131 (1971).

22. Keiichi, Koyanage, Kunio Hane and Tokio Suzuki, IEEE Trans. Electron Devices, Vol. ED 24, No. 6 672 (1977).

23. Alexander, D. R., et al., Component Statistical Characterization, AFWL-TR-80-128, Part 1-4, Air Force Weapons Laboratory, Kirtland Air Force Base, NM, September 1981.

24. Klein, N., "Electrical Breakdown in Solids," Adv. Electr. Electron Physics, L. Marton, Editor, 26, pp. 309-424, Academic Press, 1969.

25. Black, J. R., "Electromigration - A Brief Survey and Some Recent Results," IEEE Transaction on Electron Devices, Vol. 16, p. 338 (1969).

26. Davies, R. L. and F. E. Gentry, "Control of Electric Field at the Surface of p-n Junctions," IEEE Transactions on Electron Devices, ED-11, pp. 313-323, July 1963.

27. Alston, L. L., High-Voltage Technology, Oxford University Press, 1968.